

# Temperature-biased double-loop Josephson flux transducer

C. Guarcello,<sup>1,2</sup> R. Citro,<sup>1,2,3</sup> F. Giazotto,<sup>4</sup> and A. Braggio<sup>4</sup>

<sup>1</sup>*Dipartimento di Fisica “E.R. Caianiello”, Università di Salerno,  
Via Giovanni Paolo II, 132, I-84084 Fisciano (SA), Italy*

<sup>2</sup>*INFN, Sezione di Napoli Gruppo Collegato di Salerno,  
Complesso Universitario di Monte S. Angelo, I-80126 Napoli, Italy*

<sup>3</sup>*CNR-SPIN c/o Università degli Studi di Salerno, I-84084 Fisciano (Sa), Italy*

<sup>4</sup>*NEST, Istituto Nanoscienze-CNR and Scuola Normale Superiore, Piazza San Silvestro 12, I-56127 Pisa, Italy*

(Dated: January 14, 2022)

We theoretically study the behavior of the critical current of a thermally-biased tunnel Josephson junction with a particular design, in which the electrodes of the junction are enclosed in two different superconducting loops pierced by independent magnetic fluxes. In this setup, the superconducting gaps can be modified independently through the magnetic fluxes threading the loops. We investigate the response of the device as a function of the magnetic fluxes, by changing the asymmetry parameter, i.e., the ratio between the zero-temperature superconducting gaps  $\delta = \Delta_{10}/\Delta_{20}$ , and the temperatures of the two rings. We demonstrate a magnetically controllable step-like response of the critical current, which emerges even in a symmetric junction,  $\delta = 1$ . Finally, we discuss the optimal working conditions and the high response of the critical current to small changes in the magnetic flux, reporting good performances of the transducer, with a high transfer function that depends on the operating point and the quality of the junction.

## I. INTRODUCTION

Recently, several works demonstrated that a quite well-known device, a Josephson junction (JJ), can still deserve surprises when subject to a thermal gradient, i.e., unbalancing the temperatures at the two sides of the device. Thermal transport at the nanoscale and the research field of superconducting phase coherent caloritronics are attracting interest [1–10] due to the importance for the whole field of quantum technologies and quantum computing to master heat management at ultra-low temperatures. In this context, it was recently demonstrated that the Josephson transport [11–14] across a superconductor-insulator-superconductor (SIS) junction, formed by different superconductors residing at different temperatures, can show unexpected, and quite peculiar, features. For example, strong nonlinear temperature biases can induce a spontaneous breaking of the particle-hole symmetry, generating even a bipolar thermoelectric effect [15, 16]. Intriguing phenomena have been reported also in the Josephson transport, such as a steeper variation of the critical current in response to a temperature bias [11]. Surprisingly, the critical current can even increase with the temperature, thus suggesting to apply this phenomenon for a wide-band threshold calorimeter [12].

All the cases described so far, underly the importance of the alignment mechanism of the two superconducting singularities in the DOS and its anomalous components. This matching of the singularities can be triggered by different mechanisms determined by temperatures [11], biasing [15], and/or exchange fields [17].

In this work, we propose an alternative junction configuration, shown in Fig. 1, formed by enclosing a superconducting loop around each electrode, and tunneling coupling the electrodes. In this way, the magnetic

flux through these loops gives an effective way to affect the superconducting gaps. We show how to magnetically tune the step-like response of the critical current, and how the effect of a loop area asymmetry reflects on its tunability. The setup discussed in this paper can be used to control the superconducting gaps by only magnetic means in a tunnel junction. The feasibility to control thermal transport in Josephson devices via external magnetic fluxes was already extensively demonstrated in different cases [2, 18–24].

The paper is organized as follows. In Sec. II, we study the behavior of the critical current by varying the magnetic fluxes driving of the device, at different values of the ratio between the critical temperatures of the two superconductors, both in the symmetric and asymmetric case. In Sec. III, we introduce the working principles of a magnetic flux-to-critical current transducer based on a temperature-biased device, describing also a simple measurement setup. In Sec. IV, the conclusions are drawn.

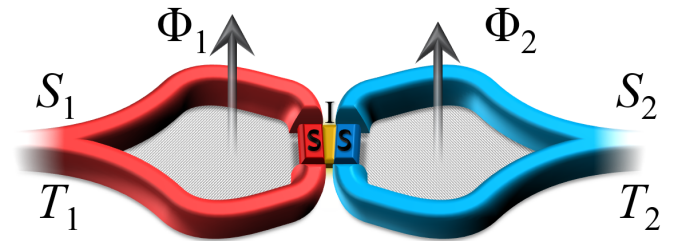


FIG. 1. Schematic of the device. The electrodes are formed by superconducting loops interrupted by small superconducting regions, which are tunnel-coupled through an insulating barrier (yellow). The left,  $S_1$ , and right,  $S_2$ , loops reside at different temperature,  $T_1$  and  $T_2$ , respectively, and are pierced by independent magnetic fluxes  $\Phi_i$  (with  $i = 1, 2$ ).

## II. THE CRITICAL CURRENT

We assume a tunnel Josephson junction (JJ) formed by different BCS superconductors  $S_1$  and  $S_2$ , with energy gaps  $\Delta_1$  and  $\Delta_2$  and residing at temperatures  $T_1$  and  $T_2$ . This device can support a Josephson current [25, 26] with a maximum value given by the relation [27–30]

$$I_c(T_1, T_2) = \frac{1}{2eR} \left| \int_{-\infty}^{\infty} \left\{ f(\varepsilon, T_1) \operatorname{Re} [\mathfrak{F}_1(\varepsilon, T_1)] \operatorname{Im} [\mathfrak{F}_2(\varepsilon, T_2)] + f(\varepsilon, T_2) \operatorname{Re} [\mathfrak{F}_2(\varepsilon, T_2)] \operatorname{Im} [\mathfrak{F}_1(\varepsilon, T_1)] \right\} d\varepsilon \right|. \quad (1)$$

Here,  $R$  is the normal-state resistance of the junction,  $f(\varepsilon, T_j) = \tanh(\varepsilon/2k_B T_j)$ , and

$$\mathfrak{F}_j(\varepsilon, T_j) = \frac{\Delta_j(T_j)}{\sqrt{(\varepsilon + i\Gamma_j)^2 - \Delta_j^2(T_j)}} \quad (2)$$

is the anomalous Green's function of the  $j$ -th superconductor [31]. We included the phenomenological Dynes parameter  $\Gamma_j = \gamma_j \Delta_{j0}$  [32], with  $\Delta_{j0} = 1.764 k_B T_{c_j}$  being the zero-temperature superconducting BCS gap [33] and  $T_{c_j}$  is the critical temperature. The Dynes parameter [32, 34] would effectively describe a lifetime broadening, and it allows to reproduce the smearing of the IV characteristics at low voltages. In fact, a non-negligible  $\gamma_j$  introduces states within the gap,  $|\varepsilon| < \Delta_j$ , in contrast with the ideal BCS case [35, 36]. In this work we assume quite good quality junctions, where  $\gamma_1 = \gamma_2 = \gamma \in [10^{-3} - 10^{-4}]$  [37–39].

According to Eq. (1), the critical current of a temperature-biased tunnel JJ depends strongly on the superconductors forming the device, so that it is useful to define a gap-asymmetry parameter

$$\delta = \frac{\Delta_{10}}{\Delta_{20}} = \frac{T_{c_1}}{T_{c_2}}. \quad (3)$$

A suitable gap-asymmetry can be eventually achieved by using electrodes formed by a proximity-coupled superconductor-normal metal bilayer, in order to fine tune the critical temperature of the film, for example by appropriately adjusting the film thickness. Unfortunately, in such a case, to change the gap asymmetry one needs to grow another sample, so the fine tuning through magnetic fluxes discussed in the following is more advantageous for experimental purposes.

For the sake of clarity, we use in this work a notation in which a tilde over a letter labels a dimensionless, normalized quantity. In particular, the quantities  $\tilde{\Phi}_j = \Phi_j/\Phi_0$  (with  $\Phi_0 = h/2e$  being the magnetic flux quantum) and  $\tilde{T}_j = T_j/\sqrt{T_{c_1} T_{c_2}}$  are the normalized magnetic flux and the normalized temperature of the  $j$ -th ring, respectively, and  $\tilde{I}_c = \frac{2eR}{\sqrt{\Delta_{10}\Delta_{20}}} I_c = 2e \frac{\sqrt{\delta R}}{\Delta_{10}} I_c$  is the normalized critical current of the device [40].

As already shown in Ref. [12], a temperature gradient across a JJ formed by different superconductors, *i.e.*, with  $\delta \neq 1$ , may affect its critical current in such a way to induce a steeper response. In particular, a critical current “jump” occurs when the electrodes reside at the temperatures at which the BCS gaps coincide and the singularities of the anomalous Green functions in the two superconductors match [31]. This phenomenon is the non-dissipative counterpart of the peaks observed in the quasiparticle charge and heat current flowing through a voltage-biased  $S_1$ -I- $S_2$  junction [31, 39, 41–44], both determined by the alignment of the gap singularities of the BCS superconductors [31]. In Ref. [12] it was demonstrated that a requirement to observe this peculiar  $I_c$  behavior is maintaining a temperature bias across the device. In other words, the fine control of temperatures is strictly necessary to observe this phenomenon. Instead, here we show how to relax this quite demanding requirement by proposing an alternative design of the device, which allows to accurately tune the superconducting gap. In fact, we demonstrate how to use magnetic fluxes, in the place of temperatures, to control the matching of singularities in the anomalous Green function, which gives rise to the critical current jumps. Moreover, the magnetic control of superconducting gaps makes it possible to observe the step-like response of  $I_c$ , only if a temperature gradient is present, even for identical zero-temperature gaps, *i.e.*,  $\delta = 1$ , in other words, in a device formed by electrodes of the same material.

The setup that we discuss in this paper is partially inspired by the superconducting quantum interference single-electron transistor (SQUSET) [45–49], which is in turn composed by two identical superconducting quantum-interference proximity transistors [50], playing respectively the role of source and drain electrodes and pierced by different magnetic fluxes. In such a setup, the superconducting rings are closed by short normal regions, where superconducting correlations affect locally the weak-link through the proximity effect. Indeed, a phase difference in the ring induces a strong modification of the spectrum of the island, where a minigap is opened [51, 52]. The loop geometry enclosing the superconducting electrode makes it possible to change the phase difference  $\varphi$  across the normal island through external magnetic fields. Thus, in the case of a short  $N$  region satisfying the condition  $E_{th} \gg \Delta$ , where  $E_{th} = \hbar D/L^2$  is the Thouless energy, with  $D$  and  $L$  being the diffusion constant and length of the region, respectively, the BCS-like spectrum with a flux-dependent induced gap reads as follow [53]

$$\Delta_j(T_j, \Phi_j) = \Delta_j(T_j) |\cos(\pi \Phi_j)|, \quad (4)$$

so that the spectral properties of the two electrodes of the tunnel JJ can be tuned via the external magnetic fluxes  $\Phi_j$  through the ring areas. Recently, a magnetometer [54] and a thermal diode [55] based on this concept were also proposed.

The crucial difference in our device, with respect a

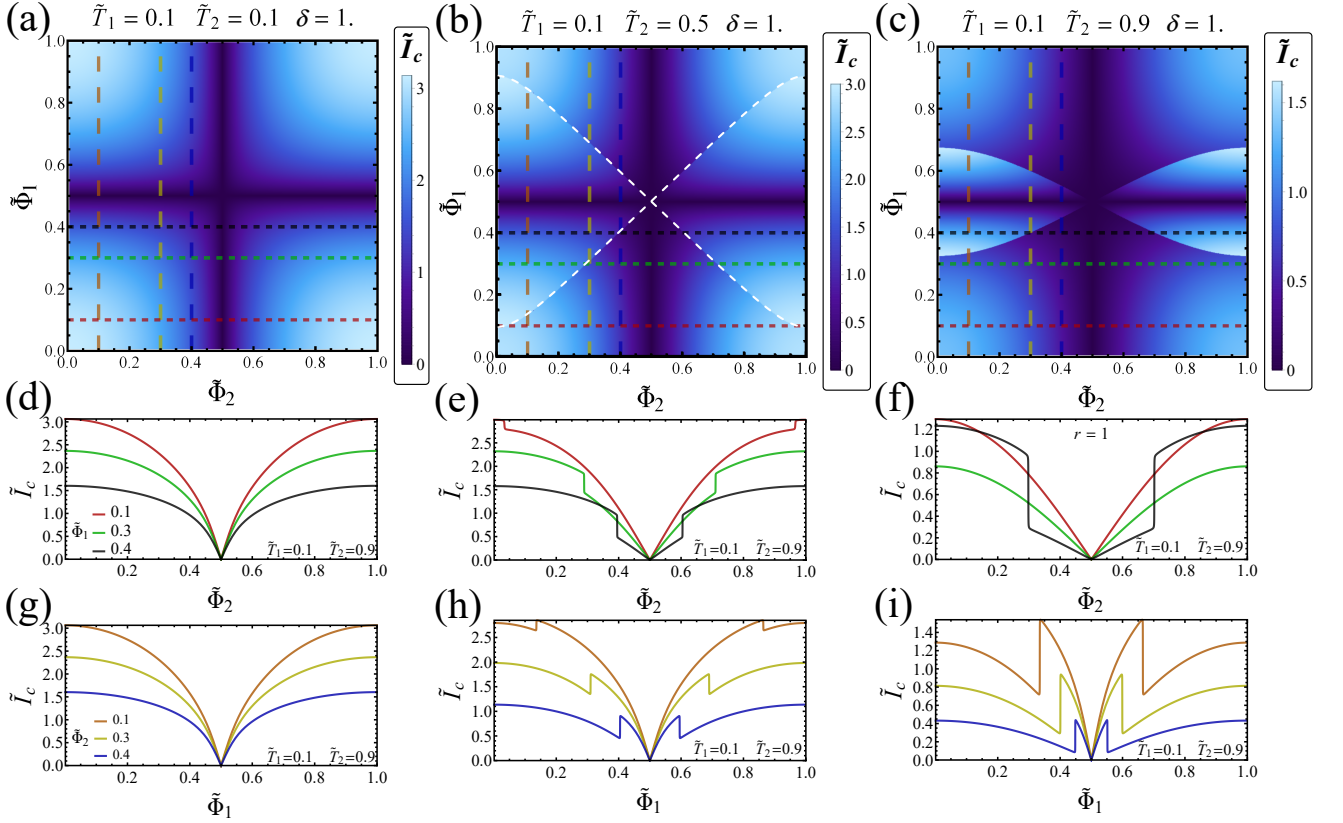


FIG. 2. Normalized critical current as a function of the normalized magnetic fluxes  $\tilde{\Phi}_1$  and  $\tilde{\Phi}_2$ , at  $\delta = 1$ ,  $\tilde{T}_1 = 0.1$ , and  $\tilde{T}_2 = 0.1, 0.5$  and  $0.9$ , see panels (a), (b), and (c), respectively. The horizontal short-dashed lines indicate the  $\tilde{\Phi}_1$  values at which the curves in panels (d), (e), and (f) are calculated, while the vertical long-dashed lines indicate the  $\tilde{\Phi}_2$  values at which the curves in panels (g), (h), and (i) are calculated. The legend in panel (d) refers also to panels (e) and (f), while the legend in panel (g) refers also to panels (h) and (i).

SQUiSET, is that the two proximized regions are tunnel-coupled through an insulating barrier, see Fig. 1, instead of being coupled to the Coulomb-blockaded island. For our setup, the critical current of the device is given by Eq. (1), but the superconducting gaps depend on the magnetic fluxes according to Eq. (4). Consequently, the dependence on the magnetic flux of the gaps is reflected first on the Green functions  $\mathfrak{F}_j$ , see Eq. (2), and then on the critical current  $I_c$ .

Assuming the independent control of the magnetic fluxes [48] or alternatively considering two different loop areas, we can investigate the system response as a function of the external magnetic flux. In this way, it is possible to observe the anomalous  $I_c$  response also when the rings are made by the same superconductor.

#### A. The symmetric-gap case ( $\delta = 1$ )

In this section we assume that the rings are made by the same superconductor, i.e.,  $\delta = 1$ . Figure 1 shows a possible experimental realization of the proposed device, where we indicate the magnetic fluxes,  $\Phi_1$  and  $\Phi_2$ , piercing the superconducting rings  $S_1$  and  $S_2$ , which reside at

temperatures  $T_1$  and  $T_2$ , respectively.

The density plots in Fig. 2 describe the behavior of the normalized critical current,  $\tilde{I}_c$ , as a function of the normalized magnetic fluxes,  $\tilde{\Phi}_1$  and  $\tilde{\Phi}_2$ , considering normalized temperatures equal to  $\tilde{T}_1 = 0.1$  and  $\tilde{T}_2 = 0.1, 0.5$ , and  $0.9$ , see panels (a), (b), and (c), respectively [56]. In all these density plots we observe that when  $\tilde{\Phi}_j = 0.5$  the critical current is totally suppressed, since in this case  $\Delta_j \rightarrow 0$ , see Eq. (4) [57].

For comparison, we report first the results obtained assuming no thermal gradient across the system, i.e.,  $\tilde{T}_1 = \tilde{T}_2 = 0.1$ , see Fig. 2(a). In this situation, a magnetic flux change produces only a modulation of  $\tilde{I}_c$  due to the gap closing, without the appearance of any jumps [see also Figs. 2(d) and (g)].

Conversely, the density plot in Fig. 2(b), which is obtained by increasing  $\tilde{T}_2$ , shows an abrupt change in color, i.e. a transition from light to dark shades of blue, which indicates a sudden change of the critical current. This phenomenon is highlighted in panel Fig. 2(e), where three selected profiles of  $\tilde{I}_c$  as a function of  $\tilde{\Phi}_2$  for different  $\tilde{\Phi}_1$ 's are shown as well. The situations plotted in this

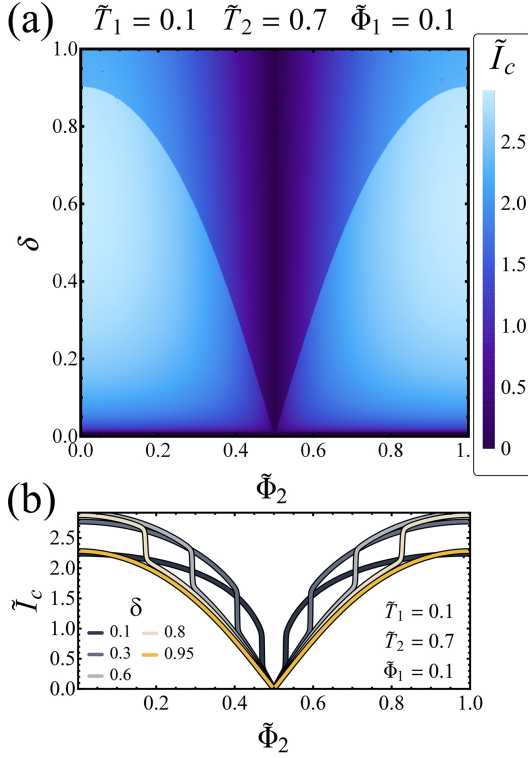


FIG. 3. (a) Normalized critical current as a function of  $\delta$  and  $\tilde{\Phi}_2$ . (b) Normalized critical current as a function of  $\tilde{\Phi}_2$  at different values of  $\delta$ . Both panels are obtained for  $\tilde{\Phi}_1 = 0.1$ ,  $\tilde{T}_1 = 0.1$ , and  $\tilde{T}_2 = 0.7$ .

figure corresponds to the horizontal short-dashed lines in Fig. 2(b). All curves show a step-like response of  $\tilde{I}_c$  at specific values of the magnetic flux  $\tilde{\Phi}_2 = \tilde{\Phi}_2^*$ . In panel (h) we show three other selected profiles of  $\tilde{I}_c$  as a function of  $\tilde{\Phi}_1$  for fixed  $\tilde{\Phi}_2$  values, which correspond to the vertical long-dashed lines in Fig. 2(b). In this case we observe a critical current jump, but these curves behave differently with respect to that in Fig. 2(e). Indeed, the profiles in Fig. 2(e) and (h), i.e.,  $\tilde{I}_c$  vs  $\tilde{\Phi}_2$  and  $\tilde{I}_c$  vs  $\tilde{\Phi}_1$ , respectively, demonstrate that  $\tilde{I}_c(\tilde{\Phi}_2^*)$  reduces at the jump, while  $\tilde{I}_c(\tilde{\Phi}_1^*)$  increases at the jump.

From the density plot in panels (b) and (c) we also note that the critical current undergoes a jump only within specific  $\tilde{\Phi}_1$  range of values. To understand why in some cases the step-like behavior does not emerge, we remind that this phenomenon stems from the alignment of the singularities in the Green's functions  $\mathfrak{F}_j$ . In other words, making explicit the magnetic flux dependence, a jump appears only when

$$\Delta_1(\tilde{T}_1) \left| \cos(\pi \tilde{\Phi}_1) \right| = \Delta_2(\tilde{T}_2) \left| \cos(\pi \tilde{\Phi}_2) \right|. \quad (5)$$

In Fig. 2(b) white dashed lines mark the  $(\tilde{\Phi}_1^*, \tilde{\Phi}_2^*)$  couples of values solving this equation; these values, i.e., the “positions” of the jumps, depend on both the working temperatures and the gap asymmetry. Conversely, for

those fluxes for which Eq. (5) cannot be satisfied, the critical current shows no jumps.

### B. The asymmetric-gap case ( $\delta \neq 1$ )

It is intriguing to discuss also how the gap asymmetry  $\delta$  affects the behavior of the critical current, i.e., assuming that the electrodes are made by different superconductors, still keeping a temperature gradient. This is illustrated in Fig. 3(a), for  $\tilde{T}_1 = 0.1$  and  $\tilde{T}_2 = 0.7$ . Here, we show how  $\tilde{I}_c$  depends on  $\delta$  and  $\tilde{\Phi}_2$ , when  $\tilde{\Phi}_1$  is kept fixed, *e.g.*,  $\tilde{\Phi}_1 = 0.1$ . We note first that for this  $\tilde{\Phi}_1$  value in the symmetric-gap case ( $\delta = 1$ )  $\tilde{I}_c$  presents no jumps, see Fig. 2. Instead, reducing the asymmetry, we can find matched cases that solve Eq. (5): in fact, below a certain  $\delta$  value, i.e.,  $\delta \lesssim 0.9$ , we observe that  $\tilde{I}_c(\tilde{\Phi}_2)$  undergoes two jumps. For strong asymmetries, *i.e.*, when  $\delta \rightarrow 0$ , the positions of these two  $\tilde{I}_c$  jumps shift towards  $\tilde{\Phi}_2 = 0.5$ . This behavior is better illustrated in Fig. 3(b), where we highlight some selected  $\tilde{I}_c(\tilde{\Phi}_2)$  profiles obtained at different  $\delta$ .

### C. The asymmetric-ring area case

In the previous sections, we assumed two independent magnetic fields piercing the superconducting rings. This strategy, although offering the control upon two independent degrees of freedom, is demanding from the point of view of the device fabrication, which has to include two independent local coils. For this reason we discuss here a simpler realization, which takes advantages on the fact that the loop areas may be different. In this way, the device can be controlled by a single magnetic field threading the areas  $A_j$  of both superconducting rings, as in the case investigated in Ref. [47]. In this case, we can conveniently define the area-asymmetry parameter

$$\alpha = \frac{A_1}{A_2} = \frac{\tilde{\Phi}_1}{\tilde{\Phi}_2}. \quad (6)$$

Once a temperature gradient is established, the only remaining control parameter is the common magnetic field piercing the superconducting ring areas, *i.e.*,  $\tilde{\Phi} = \tilde{\Phi}_1 = \alpha \tilde{\Phi}_2$ .

Figure 4 presents a collection of density plots showing the normalized critical current  $\tilde{I}_c$ , in the case of loops with different areas threatened by the same magnetic field, as a function of the control flux  $\tilde{\Phi}$  at different values of the gap asymmetry  $\delta$ . The temperature bias is kept fixed and the density plots are obtained assuming different area asymmetries  $\alpha$ . Interestingly, the condition  $\alpha = 0$  implies a zero area  $A_1$  of the ring  $S_1$ . In other words, this is equivalent to replace the loop geometry with a simple superconducting stripe for the cold electrode. On the opposite side, imposing  $\alpha = 1$  means taking two rings with the same area. Thus, density plots in Fig. 4 serve



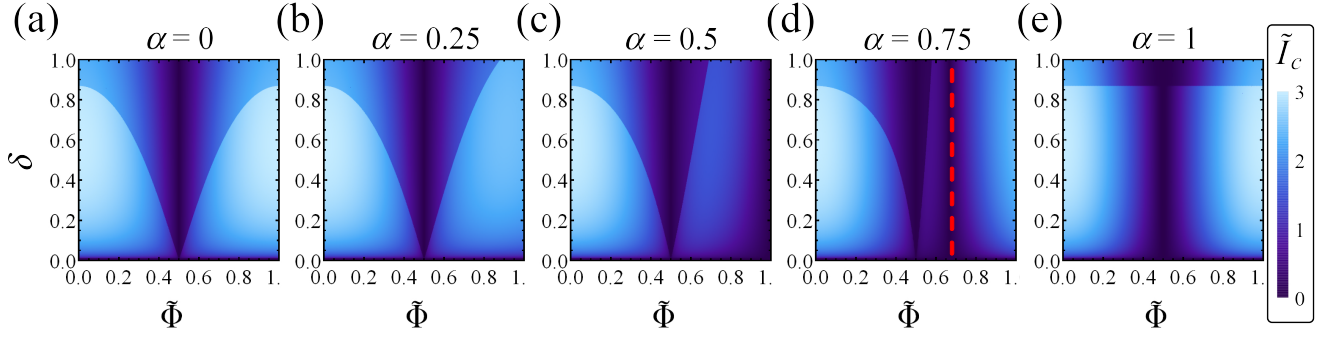


FIG. 4. Normalized critical current as a function of  $\delta$  and  $\Phi$  in the case of asymmetric area loops, with the ratio between the loops areas equal to  $\alpha = \{0, 0.25, 0.5, 0.75, 1\}$ . All panels are obtained for  $\tilde{T}_1 = 0.1$  and  $\tilde{T}_2 = 0.7$ .

to highlight the  $\tilde{I}_c(\tilde{\Phi}, \delta)$  transition from the single-loop design, see Fig. 4(a) for  $\alpha = 0$ , to the identical-loops design, see Fig. 4(e) for  $\alpha = 1$ .

We observe that even in the single-loop device the critical current behaves peculiarly, see Fig. 4(a). Then, as  $\alpha$  increases, the density plot becomes more and more asymmetric in  $\tilde{\Phi}$ . In particular, the right side of the contour plot, *i.e.*, for  $\tilde{\Phi} > 0.5$ , tends to evidently distort when  $\alpha \neq 0$ . Conversely, the left side of the contour plot, *i.e.*, for  $\tilde{\Phi} < 0.5$ , seems to be significantly affected by  $\alpha$  only when it is very close to 1. Interestingly, for  $\alpha = 0.75$  a new kink appears in the  $\tilde{I}_c$  profiles [see the red dashed line in Fig. 4(d)]. The kinks in Fig. 4 occur in correspondence of that fluxes that make the  $\cos(\pi\Phi)$  or  $\cos(\alpha\pi\Phi)$  terms zero. Thus, for  $\alpha = 0.75$  these are centered in  $\Phi = 1/2$  and  $\Phi = 1/(2\alpha) \sim 0.67$ .

Finally, in the identical-loops design, *i.e.*,  $\alpha = 1$ , no jumps are observed changing  $\tilde{\Phi}$ , see Fig. 4(e). However, in this figure, we observe a clear change in the  $\tilde{I}_c$  behavior, which is demonstrated by the light-to-dark transition of the density plot texture, at  $\delta \simeq 0.87$ . Even this threshold gap asymmetry can be evaluated as that value that satisfies Eq. (5), at a given temperature gradient.

### III. FLUX-TO-CRITICAL CURRENT RESPONSE

The physical effects described so far could promptly find an application as a high sensitivity magnetic flux-to-critical current transducer. In this section we look at the performance of the device by adjusting the system parameters. In particular, we expect the steep change in the critical current to result in a very high sensitivity for detecting small flux changes. Indeed, a tiny variation of the magnetic flux  $\tilde{\Phi}_j$  induces a huge variation of the critical current.

When the device is employed as a magnetic flux-to-current transducer, an important figure of merit is the flux-to-current transfer function, defined as the derivative of the critical current with respect to the driving

magnetic flux (critical current responsivity) [58–61]

$$\tilde{I}_{\tilde{\Phi}_j} = \left| \frac{\partial \tilde{I}_c}{\partial \tilde{\Phi}_j} \right|. \quad (7)$$

Since  $\tilde{I}_c$  and  $\tilde{\Phi}_j$  are normalized quantities, in non-normalized units the transfer function is

$$I_{\Phi_j} = \frac{1}{2e\Phi_0} \frac{\Delta_{10}}{\sqrt{\delta}R} \tilde{I}_{\tilde{\Phi}_j}. \quad (8)$$

In the case of a symmetric Nb-junction,  $T_{c1} = 9.2$  K and  $\delta = 1$ , with  $R = 10$  k $\Omega$ , one obtains  $\frac{\Delta_{10}}{2e\Phi_0\sqrt{\delta}R} \simeq 0.07$   $\mu\text{A}/\Phi_0$ , representing the unit of measure of the transfer function. Moreover, we can also investigate the height of the critical current jump,  $\Delta\tilde{I}_c$ , as a function of the various system parameters [62].

In the following, we consider a device formed by identical superconductors, *i.e.*,  $\delta = 1$ , and the independent control of the magnetic fields. We discuss only the figures of merit in the case of a monotonic variation of  $\tilde{I}_c$  at the jump, *e.g.*, the  $\tilde{I}_c$  vs  $\tilde{\Phi}_2$  curves in Fig. 2(e) [63].

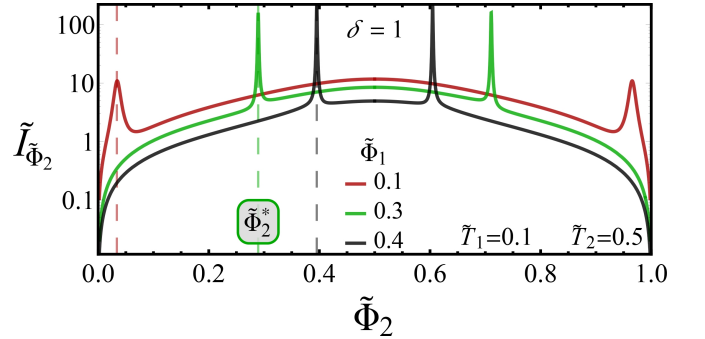


FIG. 5. Flux-to-current transfer functions  $\tilde{I}_{\tilde{\Phi}_2}$ , at  $\delta = 1$ ,  $\tilde{T}_1 = 0.1$ ,  $\tilde{T}_2 = 0.5$ , and different values of  $\tilde{\Phi}_1$ . The vertical dashed lines indicate the magnetic fluxes  $\tilde{\Phi}_2^*$  at which  $I_c$  jumps. The maximum transfer function, *i.e.*, the  $\tilde{I}_{\tilde{\Phi}_2}$  value at the  $\tilde{I}_c$  jump, approaches the values  $\tilde{I}_{\tilde{\Phi}_2}^{\max} \simeq \{11, 160, \text{ and } 220\}$  at the driving fluxes  $\tilde{\Phi}_1 = \{0.1, 0.3, \text{ and } 0.4\}$ , respectively.

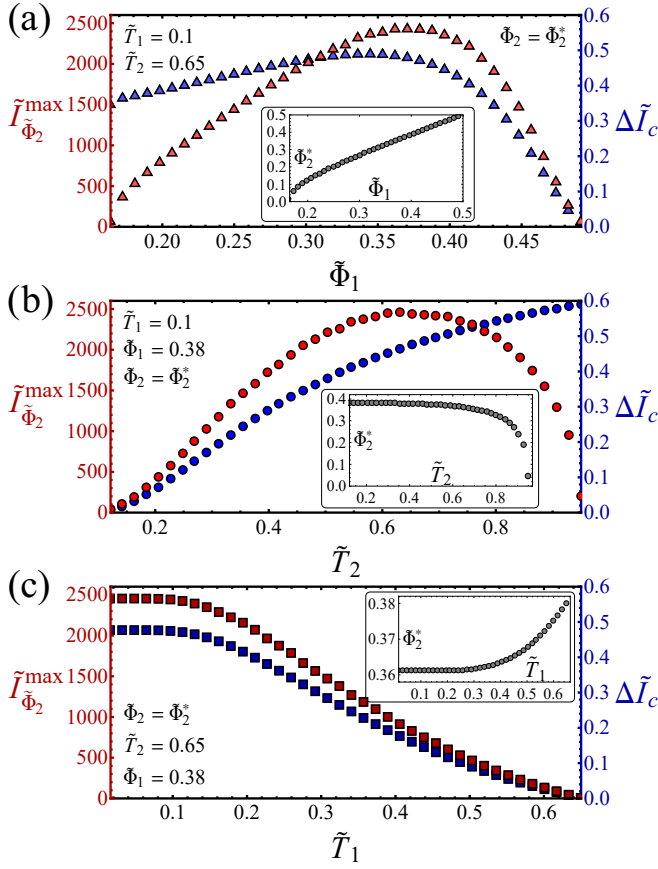


FIG. 6. Maximum flux-to-current transfer function  $\tilde{I}_{\Phi_2}^{\max}$  (left axis, red symbols) and height of the critical current jump  $\Delta\tilde{I}_c$  (right axis, blue symbols) versus: (a)  $\Phi_1$  at fixed  $\tilde{T}_2 = 0.65$  and  $\tilde{T}_1 = 0.1$ ; (b)  $\tilde{T}_2$  at fixed  $\Phi_1 = 0.38$  and  $\tilde{T}_1 = 0.1$ ; (c)  $\tilde{T}_1$  at fixed  $\Phi_1 = 0.38$  and  $\tilde{T}_2 = 0.65$ . The insets show the position,  $\Phi_2^*$ , of the  $\tilde{I}_c$  jump. The other parameters are  $\delta = 1$  and  $\gamma = 10^{-4}$ .

This means to use the magnetic flux  $\tilde{\Phi}_1$  only as a control knob to tune the position of the optimal working point of the device.

In Fig. 5 we present the  $\tilde{I}_{\Phi_2}$  profiles obtained by numerical differentiation of the data shown in Fig. 2(e). As expected, the transfer function is highly peaked in correspondence of each  $\tilde{I}_c$  jump, that is when  $\tilde{\Phi}_2 = \tilde{\Phi}_2^*$  (these values are marked by vertical dashed lines). A magnetometer done with feedback loop kept at the optimal operating point promises a very high transfer function and, correspondingly, a very high sensitivity [61].

Certainly, the height of the  $\tilde{I}_{\Phi_2}$  peaks depends on the steepness of the jump, which in turn depends on its “position”,  $\tilde{\Phi}_2^*$ , that is on the value of the driving flux  $\tilde{\Phi}_1$ . In fact, from Fig. 5(a) one could figure out that when  $\tilde{\Phi}_1$  tends to the value 0.5, also  $\tilde{\Phi}_2^* \rightarrow 0.5$ . In this case, the jump of  $\tilde{I}_c$  becomes more sharp, thus making its derivative larger. However, we can reasonably expect that  $\tilde{I}_{\Phi_2}^{\max}$

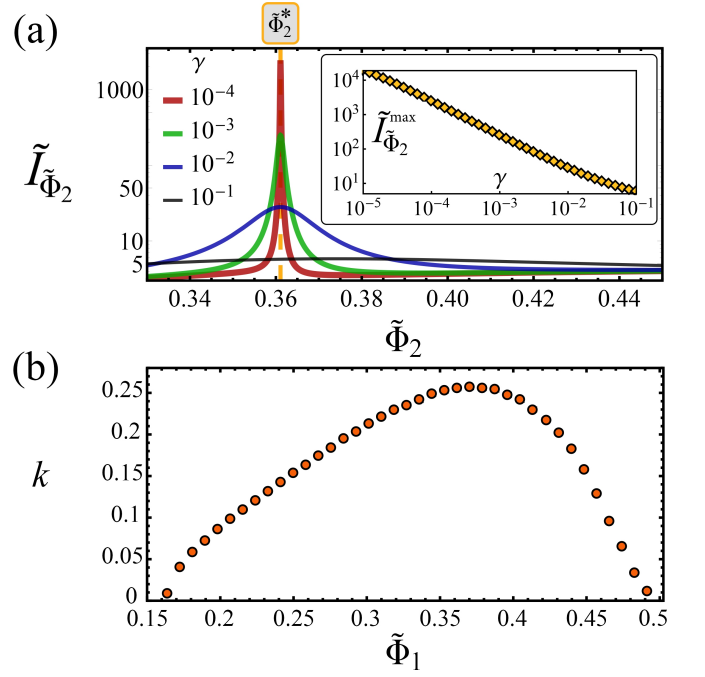


FIG. 7. Flux-to-current transfer function  $\tilde{I}_{\Phi_2}$  as a function of  $\tilde{\Phi}_2$  at different values of the Dynes parameter  $\gamma$ , at a fixed  $\tilde{\Phi}_1 = 0.38$ . The magnetic flux  $\tilde{\Phi}_2^*$  at which  $\tilde{I}_c$  shows a jump is highlighted. In the inset: Maximum flux-to-current transfer functions  $\tilde{I}_{\Phi_2}^{\max}$  (i.e., calculated at  $\tilde{\Phi}_2 = \tilde{\Phi}_2^*$ ) as a function of  $\gamma$ . (b) Fitting parameter  $k$  as a function of  $\tilde{\Phi}_1$ , see Eq. (9). The other parameters are:  $\delta = 1$ ,  $\tilde{T}_1 = 0.1$ ,  $\tilde{T}_2 = 0.65$ .

vanishes for  $\tilde{\Phi}_1 = 0.5$ , since at this magnetic flux the superconducting gap is suppressed. This suggests that one can search the optimal flux value as the  $\tilde{\Phi}_1$  value at which the sensitivity reaches a maximum. Similarly, we can look for the optimal working temperatures, such as the temperatures that maximize the sensitivity. Thus, we show in Fig. 6(a), (b), and (c) the behavior of both the maximum transfer function,  $\tilde{I}_{\Phi_2}^{\max}$ , (left axis, red symbols) and the height of the critical current jump,  $\Delta\tilde{I}_c$ , (right axis, blue symbols) as a function of  $\tilde{\Phi}_1$  (at fixed  $\tilde{T}_2 = 0.65$  and  $\tilde{T}_1 = 0.1$ ),  $\tilde{T}_2$  (at fixed  $\tilde{T}_1 = 0.1$  and  $\tilde{\Phi}_1 = 0.38$ ), and  $\tilde{T}_1$  (at fixed  $\tilde{T}_2 = 0.65$  and  $\tilde{\Phi}_1 = 0.38$ ), respectively, setting  $\delta = 1$  and  $\gamma = 10^{-4}$ .

Both  $\tilde{I}_{\Phi_2}^{\max}$  and  $\Delta\tilde{I}_c$  vs  $\tilde{\Phi}_1$ , see Fig. 6(a), behave non-monotonically. At low  $\tilde{\Phi}_1$ , the  $\tilde{I}_c$  jump is quite smooth being placed close to  $\tilde{\Phi}_2^* \sim 0$  [see the inset of Fig. 6(a)], but despite this its height  $\Delta\tilde{I}_c$  is still sizable. On the other side, for  $\tilde{\Phi}_1 \rightarrow 0.5$  the jump position tends to  $\tilde{\Phi}_2^* \rightarrow 0.5$ , so that the critical current tends to vanish due to the reduced gap, and both  $\tilde{I}_{\Phi_2}^{\max}$  and  $\Delta\tilde{I}_c$  tend to zero.

A non-monotonicity characterizes also the  $\tilde{I}_{\Phi_2}^{\max}$  vs  $\tilde{T}_2$  curve in Fig. 6(b), whereas  $\Delta\tilde{I}_c$  tends to increase with  $\tilde{T}_2$ . Clearly, both figures of merit vanish for low  $\tilde{T}_2$ 's, since

for  $\tilde{T}_2 = \tilde{T}_1$  there is no thermal gradient along the system and, thus, no critical current jump. On the other side, at large  $\tilde{T}_2$  values the jump position  $\tilde{\Phi}_2^*$  shifts towards zero, see the inset of Fig. 6(b), thus making the  $\tilde{I}_c$  step smoother, but still sizable: this is why  $\Delta\tilde{I}_c$  remains quite large even at high  $\tilde{T}_2$  values.

Finally, increasing  $\tilde{T}_1$ , see Fig. 6(c), both  $\tilde{I}_{\Phi_2}^{\max}$  and  $\Delta\tilde{I}_c$  show a plateau at low  $\tilde{T}_1$  and then reduce until vanishing for  $\tilde{T}_1 = \tilde{T}_2$ . This is clearly due the fact that lowering the thermal gradient reduces the critical current jump [11]. We observe also that the jump position  $\tilde{\Phi}_2^*$  is only weakly affected by a change of  $\tilde{T}_1$ , as shown in the inset of Fig. 6(c).

In summary, the flux-to-current transfer function  $\tilde{I}_{\Phi_2}^{\max}$  of a symmetric device, i.e., with  $\delta = 1$ , can be maximized by making the electrodes to reside at the temperatures  $\tilde{T}_2 \simeq 0.65$  and  $\tilde{T}_1 \simeq 0.1$  and setting the driving magnetic flux to the value  $\tilde{\Phi}_1 \simeq 0.38$ . In this case,  $\tilde{I}_{\Phi_2}^{\max} \sim 2500$ , that, in non-normalized units and assuming  $T_{c1} = 9.2$  K,  $\delta = 1$ ,  $R = 10$  k $\Omega$ , and  $\gamma = 10^{-4}$ , is equal to  $I_{\Phi_2}^{\max} \sim 175 \mu\text{A}/\Phi_0$  [64].

Since the sensitivity of the device essentially relies upon the sharpness of the  $\tilde{I}_c$  jump, it in turn depends also on the value of the phenomenological Dynes's parameters [12]. Thus, in Fig. 7(a) we show the behavior of  $\tilde{I}_{\Phi_2}$  vs  $\tilde{\Phi}_2$  in a neighborhood of a jump, at a few values of  $\gamma$  and  $\tilde{T}_1 = 0.1$ ,  $\tilde{T}_2 = 0.65$ , and  $\tilde{\Phi}_1 = 0.38$ . As expected, the lower  $\gamma$ , the more peaked is  $\tilde{I}_{\Phi_2}$ : in particular, as it is demonstrated clearly in the inset of Fig. 7(a), the maximum transfer function decreases by increasing  $\gamma$  as

$$\tilde{I}_{\Phi_2}^{\max} \simeq \frac{k}{\gamma} \quad (9)$$

(see Appendix A for more details about the origin of the  $1/\gamma$  dependence of the critical current responsivity). From the fit of the data in the inset of Fig. 7(a) we obtain the value  $k \simeq 0.26$ . Being the fitting coefficient  $k$  in Eq. (9) a function of the jump position, a given driving flux  $\tilde{\Phi}_1$  matches a specific value of  $k$ , see Fig. 7(b). Therefore, according to Eq. (9), an experimental measurement of the transfer function at the matching conditions could, in principle, give an estimate of the Dynes parameter  $\gamma$ .

Finally, we observe that the information content we are interested in can be extracted through a non-dispersive scheme, depicted in Fig 8, that uses a standard dc-SQUID, drawn in gray in the figure, along the lines of the readout strategy for proximity Josephson sensors discussed in Ref. [65]. In such a scheme the current flowing in the inductance  $L$  is changed when the critical current  $I_c$  in the double-ring device is modified. In fact, a constant bias current  $I_b$  divides into two parts, i.e., one flowing through the double-ring branch and the other ( $I_L$ ) through a load inductor ( $L$ ), which is mutually coupled to the dc SQUID. The variation of the critical current  $I_c$  produces a large enhancement of the Josephson

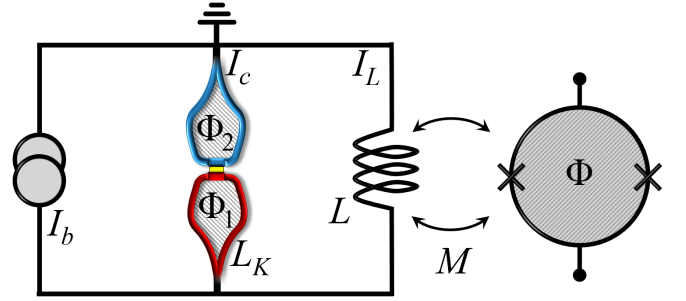


FIG. 8. Readout scheme including a dc SQUID.

kinetic inductance  $L_K = \hbar/(2eI_c)$ , which in turn results in a modification of  $I_L$ , thus producing a magnetic field which is detected by the SQUID. Other schemes, which resort to dispersive measurements, are also possible, but we do not investigate them further.

#### IV. CONCLUSIONS

In conclusion, in this paper we explored the behavior of the critical current,  $I_c$ , of a Josephson junction with a very specific design. In fact, we considered a tunnel Josephson junction formed by different superconductors, which reside at different temperatures, enclosed in two different superconducting loops, pierced by independent magnetic fluxes. These driving fluxes allow the independent control of the superconducting gaps. We discussed the behavior of  $I_c$  as a function of the driving magnetic fluxes, by changing both the temperatures of the electrodes and the ratio,  $\delta$ , between the critical temperatures of the superconductors. In particular, at a fixed temperature bias, we demonstrated the emergence of a steplike response of  $I_c$  when the system is driven by magnetic fluxes at which the BCS superconducting gaps coincide. This peculiar steplike response appears even in the symmetric junction case, that is when  $\delta = 1$ .

We also discussed the optimal working conditions to increase the transfer function of a flux-to-critical current transducer, considering also the relevant figures of merit. In this case, we also illustrated how the value of the Dynes parameter in the superconductors influences the sharpness of the  $I_c$  transition, being an important factor to increase the sensitivity.

The proposed setup can be imaged as a novel superconducting flux transducer [61], where the sensitivity to magnetic fluxes is determined by non-equilibrium temperature conditions. The feasibility of controlling the superconducting gaps, and therefore the transport properties by means of magnetic fluxes allows to relax the rather tight requirement of fine tuning of the temperatures of the two electrodes previously discussed. Indeed, once a temperature difference across the system has been established, we only need to adjust the magnetic fluxes to properly establish the operating point, so to highlight the steep jump of the critical current. Furthermore, we can

search for the best conditions that give a more abrupt response, or a more intense jump, simply by changing the magnetic flux, thus making the proposed device very appealing.

### Appendix A: Scaling of the critical current responsivity

In this section we delve into the origin of the scaling of the transfer function Eq. (9) with the Dynes parameter  $\gamma$  around the matching point. In particular, we observed that the derivative of the critical current with respect to the driving magnetic flux,  $\left| \frac{\partial I_c}{\partial \Phi_j} \right|$ , when the other magnetic flux ( $\tilde{\Phi}_i$ ) is kept fixed, scales as  $1/\gamma$  when the superconducting gaps coincide, see Eq.(4). Firstly, we note that the critical current can be written as the sum of two terms, i.e.,  $I_c(T_i, T_j) = I_{ij}(T_i) + I_{ji}(T_j)$ , with  $i, j = 1, 2$ , where

$$I_{ij}(T_i) = \frac{1}{2eR} \int_{-\infty}^{\infty} f(\varepsilon, T_i) \mathfrak{G}_{ij}(\varepsilon, \Delta_i, \Delta_j) d\varepsilon, \quad (\text{A1})$$

$f(\varepsilon, T) = \tanh(\varepsilon/2k_B T)$ , and we have defined the function  $\mathfrak{G}_{ij}(\varepsilon, \Delta_i, \Delta_j) = \text{Re}[\mathfrak{F}_i(\varepsilon, \Delta_i)] \text{Im}[\mathfrak{F}_j(\varepsilon, \Delta_j)]$  in terms of the anomalous functions given in Eq. (2).

At the matching point,  $\Delta_i = \Delta_j = \Delta$ , it is convenient to express the energies in terms of  $\Delta$ , such as  $\epsilon = \varepsilon/\Delta$ , and the current in unit of  $\Delta/(2eR)$ . In this case, the product between real and imaginary parts of the anomalous Green's functions reduces to a simple combination of Lorentzian functions:

$$\mathfrak{G}_0(\epsilon) = \frac{\gamma}{4} \left[ \frac{1}{\gamma^2 + (\epsilon - 1)^2} - \frac{1}{\gamma^2 + (\epsilon + 1)^2} \right]. \quad (\text{A2})$$

This simple expression holds only for a specific case, i.e., at the matching point, so it tells us nothing about how the critical current behaves when the gaps slightly differ, for example due to a magnetic flux modulation. To better explore this situation, it is convenient to expand  $\mathfrak{G}_{ij}$  and  $\mathfrak{G}_{ji}$  around the matching-gap condition, by setting  $\Delta_i = \Delta$  and expanding  $\Delta_j = \Delta(1 + \mathcal{D})$ . In this way, in normalized units, one can write

$$\mathfrak{G}_{ij}(\epsilon, \mathcal{D}) \simeq \mathfrak{G}_0(\epsilon) + \partial_{\mathcal{D}} \mathfrak{G}_+ \mathcal{D} \quad (\text{A3})$$

$$\mathfrak{G}_{ji}(\epsilon, \mathcal{D}) \simeq \mathfrak{G}_0(\epsilon) + \partial_{\mathcal{D}} \mathfrak{G}_- \mathcal{D} \quad (\text{A4})$$

where

$$\begin{aligned} \partial_{\mathcal{D}} \mathfrak{G}_{\pm} &= \frac{i}{4} \left( \frac{1}{\sqrt{(\epsilon + i\gamma)^2 - 1}} \pm \frac{1}{\sqrt{(\epsilon - i\gamma)^2 - 1}} \right) \\ &\times \left( \frac{(\epsilon + i\gamma)^2}{[(\epsilon + i\gamma)^2 - 1]^{3/2}} \mp \frac{(\epsilon - i\gamma)^2}{[(\epsilon - i\gamma)^2 - 1]^{3/2}} \right). \end{aligned} \quad (\text{A5})$$

Indicating, for the sake of convenience, the temperatures  $(T_i, T_j)$  as  $(T_+, T_-)$ , the critical current can be approximated as

$$I_c(T_+, T_-, \mathcal{D}) \simeq I_{c,0}(T_+, T_-) + \mathcal{D} \sum_{s=\pm} \delta I_s(T_s) + \mathcal{O}(\mathcal{D}^2), \quad (\text{A6})$$

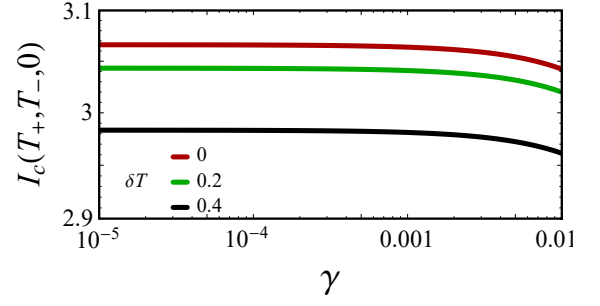


FIG. 9.  $I_c(T_+, T_-, 0)$  versus  $\gamma$ , with  $T_{\pm} = T \pm \delta T/2$ , at  $T = 0.4$  and  $\delta T = \{0, 0.2, 0.4\}$ .

where

$$I_{c,0}(T_+, T_-) = \int_{-\infty}^{\infty} \mathfrak{G}_0(\epsilon) [f(\epsilon, T_+) + f(\epsilon, T_-)] d\epsilon \quad (\text{A7})$$

$$\delta I_{\pm}(T_{\pm}) = \int_{-\infty}^{\infty} \partial_{\mathcal{D}} \mathfrak{G}_{\pm} f(\epsilon, T_{\pm}) d\epsilon. \quad (\text{A8})$$

Interestingly,  $I_c(T_+, T_-, 0)$  depends very little on  $\gamma$ , see Fig. 9 where we set  $T_{\pm} = T \pm \delta T/2$  and we vary  $\delta T$ . This behavior reflects the general fact that at the matching point the value of the critical current is weakly dependent on  $\gamma$ . See, for example, Fig. 4 of Ref. [11], where one gap deviates from the matching condition due to the temperature change of a superconducting electrode. This happens also when the variation of the gap is due to a change in the magnetic flux, see Eq. (4), as considered in the present case.

In the low-temperature limit,  $T \ll \Delta$ , the  $\tanh(\epsilon/T)$  can be approximated with the  $\text{sgn}(\epsilon)$  function, so that the integrals  $\delta I_{\pm}(T_{\pm})$  can be even solved analytically. Anyway, in the absence of a temperature gradient, i.e.,  $T_+ = T_- = T$ , one finds that  $\delta I_+(T) + \delta I_-(T) \simeq \pi/2$ . This means that the change of the critical current from the matching condition value is independent from the Dynes parameter, at least in the range of  $\gamma$  values physically relevant and considered in the manuscript.

In order to observe the steep-like behavior of  $I_c$ , a temperature gradient across the system is necessary, i.e.,  $T_+ \neq T_-$ . So, it is interesting to investigate if the presence of a temperature gradient can eventually determine also the reported  $\gamma$ -scaling. Thus, to retrieve it, we can first look separately at the behavior of the functions  $\delta I_{\pm}(T_{\pm})$ . Using again the approximation  $\tanh(\epsilon/T_{\pm}) \sim \text{sgn}(\epsilon)$  we can calculate the  $\delta I_{\pm}$  analytically, thus allowing us to immediately appreciate how they vary with  $\gamma$

$$\delta I_{\pm} \simeq \frac{1}{2\gamma} \left[ \frac{\pi\gamma - 2\gamma \tan^{-1}(\gamma)}{2} + \frac{\gamma^2 \pm 1}{\gamma^2 + 1} \right] = \frac{I_{\pm}(\gamma)}{\gamma}, \quad (\text{A9})$$

where the functions  $I_{\pm}(\gamma) \simeq 1/2 + \mathcal{O}(\gamma)^2$  are almost constant for small  $\gamma$  values (that is, in non-normalized units, for a Dynes parameter much smaller than the superconducting gaps). Finally, when adding the  $\delta I_{\pm}$  contributions into Eq. (A6), in the presence of a temperature gradient the  $1/\gamma$  scaling in the critical current survives, as

discussed in the main text. To conclude, we stress that Eq. (A9) has been derived assuming a deviation from the matching condition, regardless of what may cause this modulation. Thus, the result obtained is general, being valid whether we consider the effect of temperature [11], magnetic flux changes, or any other mechanism that could affect the superconducting gap.

## ACKNOWLEDGMENTS

F.G. acknowledges the European Research Council under Grant Agreement No. 899315-TERASEC, and the EU's Horizon 2020 research and innovation program under Grant Agreement No. 800923 (SUPERTEd) and No. 964398 (SUPERGATE) for partial financial support. A.B. acknowledges the SNS-WIS joint lab QUANTRA, funded by the Italian Ministry of Foreign Affairs and International Cooperation and the Royal Society through the International Exchanges between the UK and Italy (Grants No. IEC R2 192166 and IEC R2 212041).

- 
- [1] M. Meschke, W. Guichard, and J. P. Pekola, "Single-mode heat conduction by photons," *Nature* **444**, 187–190 (2006).
  - [2] F. Giazotto and M.J. Martínez-Pérez, "The Josephson heat interferometer," *Nature* **492**, 401–405 (2012).
  - [3] J. T. Muhonen, M. Meschke, and J. P. Pekola, "Micrometre-scale refrigerators," *Rep. Prog. Phys.* **75**, 046501 (2012).
  - [4] B. Sothmann and C. Flindt, "Quantized electronic heat flow," *Science* **342**, 569–570 (2013).
  - [5] S. Gasparinetti, K. L. Viisanen, O.-P. Saira, T. Faivre, M. Arzeo, M. Meschke, and J. P. Pekola, "Fast electron thermometry for ultrasensitive calorimetric detection," *Phys. Rev. Applied* **3**, 014007 (2015).
  - [6] A. Fornieri and F. Giazotto, "Towards phase-coherent caloritronics in superconducting circuits," *Nat. Nanotechnology* **12**, 944–952 (2017).
  - [7] J.P. Pekola and I.M. Khaymovich, "Thermodynamics in single-electron circuits and superconducting qubits," *Annu. Rev. Condens. Ma. P.* **10**, 193–212 (2019).
  - [8] S.-Y. Hwang and B. Sothmann, "Phase-coherent caloritronics with ordinary and topological Josephson junctions," *Eur. Phys. J.-Spec. Top.* **229**, 683–705 (2020).
  - [9] O. Maillet, D. Subero, J. T. Peltonen, D. S. Golubev, and J. P. Pekola, "Electric field control of radiative heat transfer in a superconducting circuit," *Nature Commun.* **11**, 4326 (2020).
  - [10] J. P. Pekola and B. Karimi, "Colloquium: Quantum heat transport in condensed matter systems," *Rev. Mod. Phys.* **93**, 041001 (2021).
  - [11] C. Guarcello, A. Braggio, P. Solinas, G. P. Pepe, and F. Giazotto, "Josephson-threshold calorimeter," *Phys. Rev. Applied* **11**, 054074 (2019).
  - [12] C Guarcello, A Braggio, P Solinas, and F Giazotto, "Nonlinear critical-current thermal response of an asymmetric Josephson tunnel junction," *Phys. Rev. Applied* **11**, 024002 (2019).
  - [13] G. Marchegiani, A. Braggio, and F. Giazotto, "Phase-tunable thermoelectricity in a Josephson junction," *Phys. Rev. Research* **2**, 043091 (2020).
  - [14] D. V. Averin, "Gap resonance in the classical dynamics of the current-biased Josephson tunnel junctions," *Phys. Rev. Research* **3**, 043218 (2021).
  - [15] G. Marchegiani, A. Braggio, and F. Giazotto, "Nonlinear thermoelectricity with electron-hole symmetric systems," *Phys. Rev. Lett.* **124**, 106801 (2020).
  - [16] G. Marchegiani, A. Braggio, and F. Giazotto, "Superconducting nonlinear thermoelectric heat engine," *Phys. Rev. B* **101**, 214509 (2020).
  - [17] G. Germanese, F. Paolucci, G. Marchegiani, A. Braggio, and F. Giazotto, "Spontaneous symmetry breaking induced thermospin effect in superconducting tunnel junctions," *Phys. Rev. B* **104**, 184502 (2021).
  - [18] A. Fornieri, C. Blanc, R. Bosisio, S. D'Ambrosio, and F. Giazotto, "Nanoscale phase engineering of thermal transport with a Josephson heat modulator," *Nature Nanotechnol.* (2015).
  - [19] C. Guarcello, P. Solinas, A. Braggio, M. Di Ventura, and F. Giazotto, "Josephson thermal memory," *Phys. Rev. Applied* **9**, 014021 (2018).
  - [20] C. Guarcello, P. Solinas, A. Braggio, and F. Giazotto, "Solitonic Josephson thermal transport," *Phys. Rev. Applied* **9**, 034014 (2018).
  - [21] C. Guarcello, P. Solinas, A. Braggio, and F. Giazotto, "Phase-coherent solitonic Josephson heat oscillator," *Sci. Rep.* **8**, 12287 (2018).
  - [22] S.-Y. Hwang, F. Giazotto, and B. Sothmann, "Phase-coherent heat circulator based on multiterminal Josephson junctions," *Phys. Rev. Applied* **10**, 044062 (2018).
  - [23] J. Senior, A. Gubaydullin, B. Karimi, J. T. Peltonen, J. Ankerhold, and J. P. Pekola, "Heat rectification via a superconducting artificial atom," *Commun. Phys.* **3**, 40 (2020).
  - [24] A. G. Bauer and B. Sothmann, "Phase-dependent transport in thermally driven superconducting single-electron transistors," *Phys. Rev. B* **104**, 195418 (2021).
  - [25] B. D. Josephson, "Possible new effects in superconductive tunnelling," *Physics Letters* **1**, 251 – 253 (1962).
  - [26] B. D. Josephson, "The discovery of tunnelling supercurrents," *Rev. Mod. Phys.* **46**, 251–254 (1974).
  - [27] A. A. Golubov, M. Yu. Kupriyanov, and E. Il'ichev, "The current-phase relation in Josephson junctions," *Rev. Mod. Phys.* **76**, 411–469 (2004).
  - [28] F. Giazotto and J. P. Pekola, "Josephson tunnel junction controlled by quasiparticle injection," *J. Appl. Phys.* **97**, 023908 (2005).
  - [29] S. Tirelli, A. M. Savin, C. Pascual Garcia, J. P. Pekola, F. Beltram, and F. Giazotto, "Manipulation and generation of supercurrent in out-of-equilibrium Josephson tunnel nanojunctions," *Phys. Rev. Lett.* **101**, 077004 (2008).
  - [30] R. Bosisio, P. Solinas, A. Braggio, and F. Giazotto, "Photonic heat conduction in Josephson-coupled



- Bardeen-Cooper-Schrieffer superconductors,” *Phys. Rev. B* **93**, 144512 (2016).
- [31] A. Barone and G. Paternò, *Physics and Applications of the Josephson Effect* (Wiley, New York, 1982).
- [32] R. C. Dynes, V. Narayanamurti, and J. P. Garno, “Direct measurement of quasiparticle-lifetime broadening in a strong-coupled superconductor,” *Phys. Rev. Lett.* **41**, 1509–1512 (1978).
- [33] M. Tinkham, *Introduction to Superconductivity*, Dover Books on Physics Series (Dover Publications, 2004).
- [34] R. C. Dynes, J. P. Garno, G. B. Hertel, and T. P. Orlando, “Tunneling study of superconductivity near the metal-insulator transition,” *Phys. Rev. Lett.* **53**, 2437–2440 (1984).
- [35] J. P. Pekola, V. F. Maisi, S. Kafanov, N. Chekurov, A. Kemppinen, Yu. A. Pashkin, O.-P. Saira, M. Möttönen, and J. S. Tsai, “Environment-assisted tunneling as an origin of the Dynes density of states,” *Phys. Rev. Lett.* **105**, 026803 (2010).
- [36] O.-P. Saira, A. Kemppinen, V. F. Maisi, and J. P. Pekola, “Vanishing quasiparticle density in a hybrid Al/Cu/Al single-electron transistor,” *Phys. Rev. B* **85**, 012504 (2012).
- [37] J. P. Pekola, T. T. Heikkilä, A. M. Savin, J. T. Flyktman, F. Giazotto, and F. W. J. Hekking, “Limitations in cooling electrons using normal-metal-superconductor tunnel junctions,” *Phys. Rev. Lett.* **92**, 056804 (2004).
- [38] M. J. Martínez-Pérez, A. Fornieri, and F. Giazotto, “Rectification of electronic heat current by a hybrid thermal diode,” *Nature Nanotechnol.* **10**, 303–307 (2015).
- [39] A. Fornieri, G. Timossi, R. Bosisio, P. Solinas, and F. Giazotto, “Negative differential thermal conductance and heat amplification in superconducting hybrid devices,” *Phys. Rev. B* **93**, 134508 (2016).
- [40] The normalization with respect to the geometric mean of the critical temperatures,  $\sqrt{T_{c1}T_{c2}}$ , is convenient to treat asymmetric systems. Thus, the condition  $T_1 = T_2$ , *i.e.*, the absence of a temperature gradient, corresponds to  $\tilde{T}_1 = \tilde{T}_2$ , regardless of the value of  $\delta$ . Anyway, in the case of asymmetric gaps, there are some constraints on the admissible normalized temperatures to keep both electrodes superconducting, that is  $\tilde{T}_1 \leq \sqrt{\delta}$  and  $\tilde{T}_2 \leq 1/\sqrt{\delta}$ .
- [41] S. Shapiro, P. H. Smith, J. Nicol, J. L. Miles, and P. F. Strong, “Superconductivity and electron tunneling,” *IBM J. Res. Dev.* **6**, 34–43 (1962).
- [42] P. Townsend and J. Sutton, “Investigation by electron tunneling of the superconducting energy gaps in Nb, Ta, Sn, and Pb,” *Phys. Rev.* **128**, 591–595 (1962).
- [43] R. E. Harris, “Cosine and other terms in the Josephson tunneling current,” *Phys. Rev. B* **10**, 84–94 (1974).
- [44] D. Golubev, T. Faivre, and J. P. Pekola, “Heat transport through a Josephson junction,” *Phys. Rev. B* **87**, 094522 (2013).
- [45] J. J. Vartiainen, M. Möttönen, J. P. Pekola, and A. Kemppinen, “Nanoampere pumping of Cooper pairs,” *Appl. Phys. Lett.* **90**, 082102 (2007).
- [46] E. Enrico and F. Giazotto, “Superconducting quantum interference single-electron transistor,” *Phys. Rev. Applied* **5**, 064020 (2016).
- [47] E. Enrico, E. Strambini, and F. Giazotto, “Phase-driven charge manipulation in hybrid single-electron transistor,” *Sci. Rep.* **7**, 13492 (2017).
- [48] E. Enrico, L. Croin, E. Strambini, and F. Giazotto, “On-chip tuning of electrodes quasiparticles population in fully superconducting squisets,” (2019), arXiv:1901.01248 [cond-mat.supr-con].
- [49] A. Greco, L. Fasolo, V. Marino, and E. Enrico, “Flux pumping of Cooper pairs through a Josephson energy-suppression pump,” (2021), arXiv:2109.13758 [cond-mat.supr-con].
- [50] F. Giazotto, J. T. Peltonen, M. Meschke, and J. P. Pekola, “Superconducting quantum interference proximity transistor,” *Nature Physics* **6**, 254–259 (2010).
- [51] T. T. Heikkilä, J. Särkkä, and Frank K. Wilhelm, “Supercurrent-carrying density of states in diffusive mesoscopic Josephson weak links,” *Phys. Rev. B* **66**, 184513 (2002).
- [52] H. le Sueur, P. Joyez, H. Pothier, C. Urbina, and D. Esteve, “Phase controlled superconducting proximity effect probed by tunneling spectroscopy,” *Phys. Rev. Lett.* **100**, 197002 (2008).
- [53] F. Giazotto and F. Taddei, “Hybrid superconducting quantum magnetometer,” *Phys. Rev. B* **84**, 214502 (2011).
- [54] L. Fasolo, D. Borchia, and E. Enrico, “Magnetic flux sensing exploiting two SQUITs connected by means of a floating island,” *IEEE T. Appl. Supercon.* **31**, 1–4 (2021).
- [55] D. Goury and R. Sánchez, “Reversible thermal diode and energy harvester with a superconducting quantum interference single-electron transistor,” *Appl. Phys. Lett.* **115**, 092601 (2019).
- [56] We note that for  $\delta = 1$  both temperatures are normalized to the same critical temperature, *i.e.*,  $\tilde{T}_j = T_j/T_c$  with  $j = 1, 2$ .
- [57] This is a clear consequence of the fact that, in general, according to the Ambegaokar-Baratoff relation [66] the critical current is proportional to  $I_c \propto \sqrt{\Delta_{10}\Delta_{20}}$ .
- [58] R. Russo, C. Granata, P. Walke, A. Vettoliere, E. Esposito, and M. Russo, “NanoSQUID as magnetic sensor for magnetic nanoparticles characterization,” *J. Nanopart. Res.* **13**, 5661–5668 (2011).
- [59] R. Russo, C. Granata, E. Esposito, D. Peddis, C. Cannas, and A. Vettoliere, “Nanoparticle magnetization measurements by a high sensitive nano-superconducting quantum interference device,” *Appl. Phys. Lett.* **101**, 122601 (2012).
- [60] E. Esposito, C. Granata, M. Russo, R. Russo, and A. Vettoliere, “High sensitive magnetic nanosensors based on superconducting quantum interference device,” *IEEE T. Magn.* **49**, 140–143 (2013).
- [61] C. Granata and A. Vettoliere, “Nano superconducting quantum interference device: A powerful tool for nanoscale investigations,” *Phys. Rep.* **614**, 1–69 (2016).
- [62] The height of the critical current jump,  $\Delta\tilde{I}_c$ , is obtained estimating first the full width at half maximum,  $2\phi$ , of the Lorentzian function used to fit the  $|\partial\tilde{I}_c/\partial\tilde{\Phi}_j|$  profile around a peak, and then as the absolute value of the difference between the  $\tilde{I}_c(\tilde{\Phi}_j)$  values calculated at a distance  $\pm 3\phi$  from the  $\tilde{I}_c$  jump position,  $\tilde{\Phi}_j^*$ , that is  $\Delta\tilde{I}_c = |\tilde{I}_c(\tilde{\Phi}_j^* - 3\phi) - \tilde{I}_c(\tilde{\Phi}_j^* + 3\phi)|$ .
- [63] We observe that in the case of a non-monotonic  $\tilde{I}_c$ , *e.g.*,  $\tilde{I}_c$  vs  $\tilde{\Phi}_1$  curves in Fig. 2(h), the  $\tilde{I}_c$  slope changes around a jump and thus we expect a multi-peaked  $\tilde{I}_{\tilde{\Phi}_1}$  transfer function, even crossing zero around the peak. This is why, in view of a flux-to-current transducer, we focus only on

- the analysis of the single-peaked transfer function,  $\tilde{I}_{\Phi_2}$ .
- [64] We additionally stress that the sensitivity can be further optimized by assuming an asymmetric device, that is made by different superconductors. In fact, the value  $\tilde{I}_{\Phi_2}^{\max} \sim 3400$ , corresponding to  $I_{\Phi_2}^{\max} \sim 240\mu\text{A}/\Phi_0$ , is reached in the case of  $\delta = 0.4$ , assuming optimal values for the other parameters (plot not shown).
- [65] F. Giazotto, T. T. Heikkilä, G. P. Pepe, P. Helistö, A. Luukanen, and J. P. Pekola, “Ultrasensitive proximity Josephson sensor with kinetic inductance readout,” *Appl. Phys. Lett.* **92**, 162507 (2008).
- [66] V. Ambegaokar and A. Baratoff, “Tunneling between superconductors,” *Phys. Rev. Lett.* **10**, 486–489 (1963).